Research Article

Hot-nanoparticle-mediated fusion of selected cells

Azra Bahadori[1,2], Lene B. Oddershede[1,2] (✉), and Poul M. Bendix[1] (✉)

[1] *Blegdamsvej 17, Niels Bohr Institute, University of Copenhagen, 2100 Copenhagen, Denmark*
[2] *Lundbeck Foundation Center for Biomembranes in Nanomedicine, University of Copenhagen, 2100 Copenhagen, Denmark*

ABSTRACT

Complete fusion of two selected cells allows for the creation of novel hybrid cells with inherited genetic properties from both original cells. Alternatively, via fusion of a selected cell with a selected vesicle, chemicals or genes can be directly delivered into the cell of interest, to control cellular reactions or gene expression. Here, we demonstrate how to perform an optically controlled fusion of two selected cells or of one cell and one vesicle. Fusion is mediated by laser irradiating plasmonic gold nanoparticles optically trapped between two cells (or a vesicle and a cell) of interest. This hot-particle-mediated fusion causes total mixing of the two cytoplasms and the two cell membranes resulting in formation of a new hybrid cell with an intact cell membrane and enzymatic activity following fusion. Similarly, fusion between a vesicle and a cell results in delivery of the vesicle cargo to the cytoplasm, and after fusion, the cell shows signs of viability. The method is an implementation of targeted drug delivery at the single-cell level and has a great potential for cellular control and design.

1 Introduction

Membrane fusion is a critical step in many biological processes, for instance, during fertilization where the oocyte fuses with sperm cells, or in the synaptic region, where neuronal signaling relies on protein-mediated budding and fusion of vesicles. A prerequisite for membrane fusion is that the membranes be brought into close contact; the presence of bulky membrane proteins or a thin layer of water may prevent fusion [1]. When two bilayers are adjacent, fusion does not happen spontaneously due to the high energy barriers associated with intermembrane repulsion and with the formation of high membrane curvature during stalk-and-fusion pore formation. These energy barriers can be overcome by proteins that mediate *in vivo* fusion, for instance, by the calcium-triggered soluble *N*-ethylmaleimide-sensitive-factor attachment protein receptor (SNARE) protein complexes, which facilitate fusion in the synaptic region [2]. Protein-mediated membrane fusion may share common principles because different fusogenic proteins share certain structural features, for example, the *Caenorhabditis elegans* cell–cell fusion protein EF-1 has been shown to be structurally homologous to viral fusion proteins [3].

The mechanism behind protein-mediated membrane fusion has been extensively studied using model membrane systems with fusogenic proteins [4–6],

---

peptides [7, 8], or by means of other agents as, e.g., certain non-steroidal anti-inflammatory drugs [9] or divalent cations [7, 10, 11]. The importance of achieving a small intermembrane distance in fusion is demonstrated in model systems by using complementary DNA strands linked to the two membranes, and by zipping the complementary strands together, the membrane separation was minimized, which favored fusion [12, 13].

Another way to fuse membranes is by electrofusion. Giant Unilamellar lipid Vesicles (GUVs) which are exposed to an electric field undergo rapid fusion of the membranes and mixing of the two lumens [14]. In addition, GUVs have been fused to cells by exposure to an AC field followed by exposure to a DC pulse, resulting in a transfer of the GUVs' lumen into the cellular cytoplasm [15].

The above-mentioned fusion methods are rather nonspecific with respect to which cells or vesicles fuse with each other. Other methods do provide some control over which populations within a sample can be selected for fusion: Using microfluidics, it is possible to trap GUVs and perform electrofusion of trapped GUVs [16]; however, researchers cannot control which GUVs will enter the microfluidic trap. Another method based on laser irradiation of gold nanoparticles (AuNPs) was recently developed to facilitate fusion between two types of cells. This method involves pulsed laser irradiation of bispecific metallic nanoparticles specifically conjugated to both types of cells. Upon pulsed laser irradiation of the nanoparticles linking the cells, cell-fusion proceeds and a hybrid cell is formed [17]. This method requires a high density of small nanoparticles conjugated to the cellular membranes, and moreover, the method does not allow for specific selection of cells to be fused, but rather utilizes existing random contacts between cells.

Recently, an approach was developed that enabled fusion between selected GUVs [18]. This facile method allowed for selection of individual GUVs labeled with distinct colors and which were suspended in a microscope chamber. Both content transfer and lipid mixing were investigated and furthermore the method allowed transfer of proteins between the lumens of the GUVs.

Here, we demonstrate how to select and completely fuse two living cells, both their cytoplasms and membranes by laser irradiating a gold nanoparticle located between the cells. By this fusion process, a syncytium is created with two nuclei and a cytoplasm that consists of a mixture of the cytoplasms of the two original cells. The new cell stays viable with a healthy metabolism for at least 4 h after fusion which was verified by testing both esterase and metabolic activity using calcein acetoxymethyl (calcein AM) and 3-(4,5-dimethylthiazol-2-yl)-2,5-diphenyltetrazolium bromide (MTT), respectively. This membrane fusion, mediated by an optically trapped hot nanoparticle [19], is a general method that allows for fusing both cells and reconstituted membranes. Finally, we also demonstrate fusion of a selected living cell with a selected GUV, which allows delivering the cargo of the GUV to the cytoplasm of the cell.

2　Experimental

2.1　Optics

The optical trapping and confocal visualization were performed by means of a Leica SP5 confocal microscope into which an optical trap based on a 1,064-nm laser (Spectra Physics J201-BL-106C) was implemented, details on the equipment are given in Ref. [20]. The laser was operated with output power of 250–750 mW in the sample. A Leica PL APO, NA = 1.2, 63× water immersion objective was used to visualize the sample and for focusing the trapping laser beam. In order to maximize the strength of the optical trap the collar of the microscope objective was adjusted to minimize spherical aberration [21]. The microscope was equipped with a piezoelectric stage (PI 731.20, Physik Instrumente, Germany) which allows for lateral movement of the sample with respect to the optical trap with nanometer precision. A glass bottom Petri-dish containing the cells, GUVs, and AuNPs was mounted on the microscope and kept at 37 °C during the experiment. The vybrant® DiO, *FAST*-DiO, calcein, and calcein AM fluorophores were excited using a 488-nm laser, the emitted intensity was collected in the spectral range 500–577 nm. A 633-nm laser line was used to excite vybrant® DiD and the emitted intensity was collected in the spectral range 640–759 nm. A 476-nm argon laser line was used

to visualize the reflection from the AuNPs, which was collected in the spectral range 465–483 nm. Formation of intracellular granular MTT formazan during metabolic activity could be clearly imaged by transmitted-light microscopy due to the high absorption by the granules.

2.2 Cell culture, fluorescent labeling, and sample preparation

Human embryonic kidney cells (HEK293, ATTC; CRL-1573) were cultured in DMEM (Gibco; supplemented with 10% (v/v) Fetal Bovine Serum (FBS), 1% PenStrep) in T25 tissue culture flasks (BD Falcon) at 37 °C in a 5% CO_2 incubator. The HEK293 cells were incubated for 5 min with trypsin to detach them from the T25 flasks. Next, the cells were washed twice with Dulbecco's phosphate-buffered saline (DPBS) buffer to minimize the toxic effects of the trypsin. They were then resus-pended in a CO_2-independent medium, containing phenol red free DMEM (Gibco; [+] 25 mM HEPES), and transferred to a Petri dish with α-casein (Sigma Aldrich C6780) coating. The cells were incubated for ~30 min inside the Petri dishes (37 °C) to let them attach to the surface.

All the cells used here were at passages 2–14. Half of the cells were labeled with vybrant® DiD and the other half with vybrant® DiO (both from Life Technologies vybrant® multicolor cell-labeling kit), their nonradiative energy transfer is minimal because these two dyes have almost no spectral overlap.

Calcein AM (Life Technologies; C3100MP) was used for the viability assay. The stock calcein AM powder was dissolved in anhydrous dimethyl sulfoxide (DMSO) and diluted in phenol-red-free DMEM (Gibco; [+] 25 mM HEPES) to a final volume fraction of DMSO in the sample of 0.0085% (v/v). Calcein AM solution was delivered to the sample via a 100 μm microfilament coupled to a syringe. For the cell–cell fusion viability studies, glass bottom microwell Petri dishes (MatTek Corporation, P35G-1.5-20-C) were incubated overnight with 2 g·L^{-1} α-casein from bovine milk. For the cell–GUV fusion viability studies, the Petri dishes were incubated overnight with a mixture of 50% (v/v) 2 g·L^{-1} α-casein and 50% (v/v) Gelatin (ES-006-B | EmbryoMax® 0.1% Gelatin Solution).

Metabolic activity in fused syncytia was also tested by adding MTT to the sample. A final concentration of 156 μg·mL^{-1} was used in the sample and the fused and unfused cells were monitored over time, using transmitted light. All experiments were done at 37 °C.

2.3 Gold nanoparticles

For cell–cell fusion experiments, 350 μL of the stock solution of 150-nm AuNPs (BBI solution; EM.GC150, $c_{150nm} = 2.8 \times 10^{-11}$ M) was added to 670 μL of the cell solution in the Petri dish. For cell–GUV fusion, 75 μL of the stock solution of 80-nm Streptavidin-coated AuNPs (NANOPARTZ™; C11-80-TS-50, $c_{80nm} = 1.8 \times 10^{-9}$ M) was incubated with GUVs containing a trace amount of biotinylated lipids (see below) for 1 h under gentle mixing prior to the fusion experiment.

2.4 GUV formation

The GUVs were made by standard electroformation using a mixture of fluid-phase DOPC lipids (1,2-dioleoyl-*sn*-glycero-3-phosphocholine, Avanti polar lipids) and DOPS lipids (1,2-dioleoyl-sn-glycero-3-phosphoserine, Avanti polar lipids) dissolved in chloro-form. The molar percentage of DOPS varied between 0% and 20%, we found that changing the percentage of the negatively charged DOPS within this range did not influence the probability of fusion. Furthermore, the GUVs contained 0.5 mol.% of the lipophilic tracer *FAST*-DiO (3,3′-dilinoleyloxacarbocyanine perchlorate, Invitrogen). For the cell–GUV fusion experiments 1 mol.% DSPE-PEG(2000) Biotin (1,2-distearoyl-*sn*-glycero-3-phosphoethanolamine-N-[biotinyl(polyethylene glycol)-2000], Avanti Polar Lipids, item 880129C) was mixed with the lipids. The vesicles were loaded with 300 or 200 mM sucrose.

3 Results and discussion

3.1 Complete fusion of selected cells

To visually distinguish two fusing cells, we labeled one population of HEK293 cells with vybrant® DiO (green) fluorophore and another population with vybrant® DiD (red) fluorophore. The two populations were mixed into a chamber which was mounted on a confocal

microscope with an optical trap implemented, thus allowing for simultaneous visualization and manipulation. The optical trap was based on a 1,064-nm laser, and details of the experimental setup and procedures are given in the Experimental section and in Ref. [20]. To avoid too firm attachment of the cells to the sample chamber, the glass surface was passivated with α-casein overnight. We never observed a spontaneous fusion of two cells within the sample, not even when the trapping laser was turned on and two cells were trapped, brought into close contact and continuously irradiated by the laser trap. Nonetheless, when AuNPs were flushed into the chamber, these were attracted by the optical trap and positioned themselves at the focus of the laser trap [22]. Such intense laser irradiation can cause significant heating of the particles, up to hundreds of degrees Celsius [23, 24]. When the laser trap was focused at the contact zone between two cells, it took tens of seconds before a AuNP diffused into the laser beam and the resulting heating caused a visible fusion of the two cells. The scattering signal from the trapped AuNP was most often consistent with the presence of a single AuNP in the trap. Occasionally, we noticed from the scattering signal that two or more nanoparticles aggregated in the trap, but the probability of this event was kept low by using a low concentration of nanoparticles. A cartoon of this process is shown in Fig. 1(a) and images from experiments are shown in Fig. 1(b). In the experiments, we selected one green and one red HEK cell (those in the dashed yellow circle) and irradiated AuNPs (150 nm in diameter, white arrow in Fig. 1(b)) in the contact zone between the cells. Complete fusion of the two cytoplasms was clearly visible because the green- and red-stained cytoplasmic lipid structures mixed, and the cell membranes clearly fused too. Figure 1(c) shows the evolution of green and red fluorescence of a certain area of the cell membrane during fusion, the average pixel fluorescence of each fluorophore drops as the cells' plasma membranes mix and the fluorophores are spread over a larger area. In the experiment shown in Fig. 1, the laser power in the sample was ~350 mW corresponding to an AuNP temperature increase (above room temperature) of ~100 °C [23, 24]. Another example of a fusion event is shown in Fig. S1 in Electronic Supplementary Material (ESM), which shows that the cytoplasm contents progressively mix and on longer time scales, ~45 min after fusion, the fluorescent cytoplasmic structures spatially overlap and start appearing yellow (instead of distinctly red and green). The two nuclei of the newly formed syncytium are distinctly visible at all times after fusion.
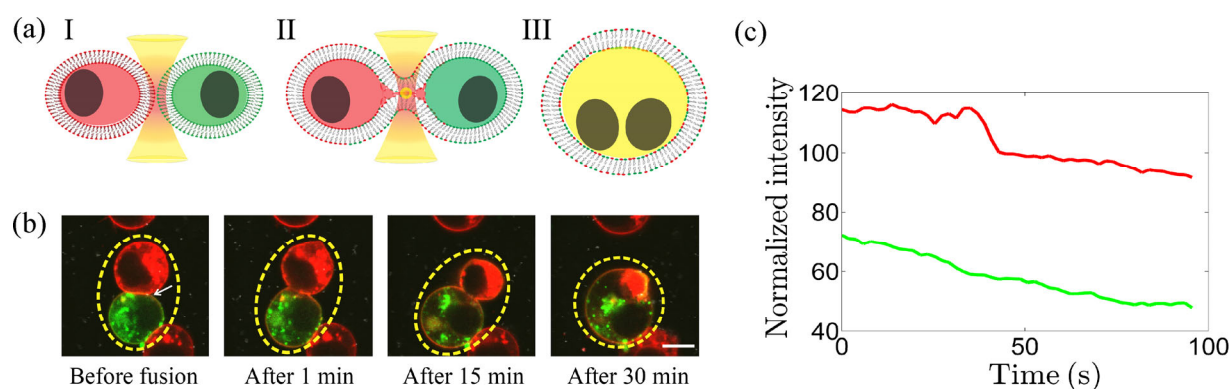

Figure 1 Cell–cell fusion mediated by optically heated AuNPs. (a) Schematic illustration of the fusion process, nuclei are drawn as black ellipsoids: (I) Two cells of interest are selected and placed next to each other using optical traps, (II) an AuNP (d_{AuNP} = 150 nm) diffuses into the optical trap located at the contact zone between the two cells, the released heat catalyzes the fusion process, (III) the cells fully fuse whereby their cell membranes and cytoplasmic contents mix. (b) Time series of confocal images of AuNP-mediated fusion between two selected cells (inside the yellow dashed ellipse), laser power at the sample was 350 mW. The cell membranes are fluorescently labeled with lipophilic fluorophores vybrant® DiD (red) and vybrant® DiO (green), respectively. A 150-nm AuNP is visible as a bright spot in the contact zone (white arrow). Scale bar is 10 μm. (c) Decrease of red and green fluorescence in a constant area within the contact zone during the fusion process (at t ~ 35 s), a result of a fixed number of fluorophores diffusing over a larger area. A total of 16 cell–cell fusions were performed.

3.2 Viability after cell–cell fusion

Cell–cell fusion can be a rather invasive event for a living cell, and to investigate the viability of the newly formed syncytium, we monitored the fused syncytium using standard cell viability assays [25–28]. To this end, we added calcein AM to the chamber, and because the plasma membrane is permeable to the non-fluorescent calcein AM, it diffused into the cytoplasm. Living cells contain active esterases which convert nonfluorescent calcein AM to green fluorescent calcein by hydrolyzing the acetoxymethyl ester bond of calcein AM [25, 26]. As cell membranes are impermeable to fluorescent calcein, this fluorescent molecule is trapped inside the cytoplasm and its presence in the cytoplasm can be used as a marker of cell viability [26]. In the experiments, we observed successful conversion of calcein AM to fluorescent calcein in the formed syncytium (up to the longest observation period, which was 2 h after the fusion event). Figures 2(a) and 2(b) show two examples of viability measurements after fusion (Fig. 2(b) shows later time frames of the experi-

ment depicted in Fig. 1(b)). A schematic illustration of the viability experiment is shown in Fig. 2(c). The presence of fluorescent calcein inside the syncytium clearly indicates that the syncytium is alive 2 h after the fusion. The fluorescence intensity of cytoplasmic calcein in the experiment is shown in Figs. 2(a) and 2(b) and is quantified in Fig. 2(d). In this graph, time zero indicates the time at which calcein AM is added to the chamber. Thus, on a time scale of a few minutes, calcein AM diffuses across the cell membrane and is converted into fluorescent calcein. In the experiment depicted in Fig. 2(a), an unfused control cell is visible above the blue dashed ellipse, this control cell also turns green upon addition of calcein AM to the chamber, and the cytoplasmic intensity of fluorescent calcein is similar to the intensity within the fused syncytium. It is, however, not a general feature that all control cells within a sample express a similar level of calcein fluorescence. This may be because the metabolic activity of a cell is coupled to the cell cycle and the cells within a sample are not synchronized. To quantitatively compare calcein fluorescence in the
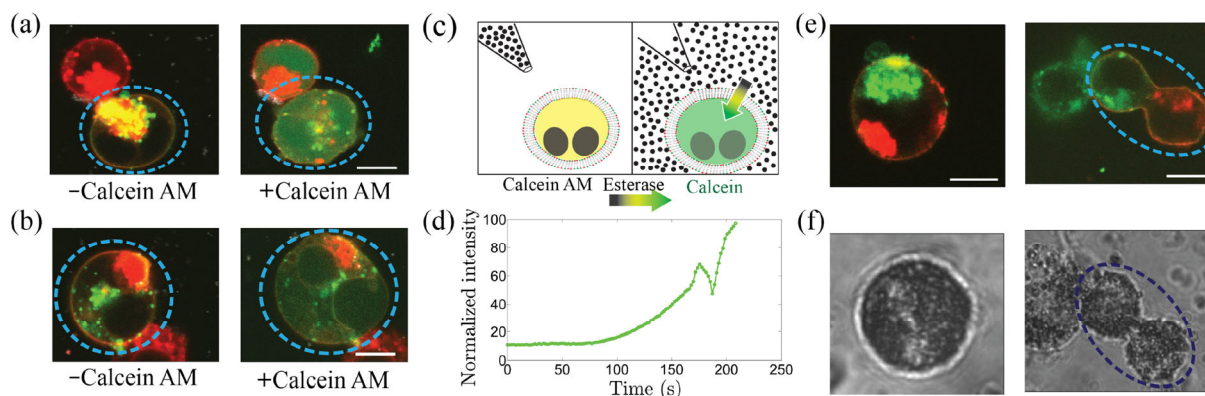
Figure 2 Viability after cell–cell fusion. (a) and (b) show images from two representative viability experiments, the green cell is labeled with vybrant® DiO and the red cell is labeled with vybrant® DiD. After fusion of the cells inside the blue ellipse, calcein AM was flushed into the sample and penetrates the cell membranes. If a cell is alive, esterases convert non-fluorescent calcein AM to fluorescent calcein, which cannot penetrate the cell membrane. d_{AuNP} = 150 nm, laser powers used: P = 250 mW for (a) and P = 350 mW for (b) in the sample, respectively. The scale bars are 10 μm. (c) Schematics showing the calcein AM viability assay. Calcein AM molecules are depicted as black solid circles which easily penetrate the cell membrane and become converted in the cytoplasm by esterases to green fluorescent calcein (shown as green color in the cytoplasm). (d) Intensity emitted after cytoplasmic enzymatic conversion of calcein AM to its fluorescently active form, calcein, in the experiment depicted in (a). Time zero corresponds to the time point when calcein AM is added to the chamber: ~2 h after fusion. Cells were tested for viability using calcein AM in seven fusion experiments. (e) and (f) Viability of fused syncytia was also demonstrated by reduction of MTT to formazan thus indicating metabolic activity of the fused structure. Confocal images are shown in (e) of the fused cells labeled with vybrant® DiO (green) and vybrant® DiD (red), respectively, and transmitted light is used in (f) to detect the dense granular aggregation of intracellular formazan. The images were acquired 4 h after the fusion event. Three fusion events were tested with MTT and all showed a similar change in contrast (see also Fig. S2 in the ESM). Scale bars in (e) are 10 μm.

syncytium cytoplasm to fluorescence in the cytoplasm of non-fused control cells, we calculated the ratio between the fluorescence of the syncytium and the average calcein fluorescence from all imaged control cells, $<I_{fused}>/<I_{unfused}>$. The intensity of fused cells tested with calcein AM was 34 ± 38 ($N = 7$ cells; mean $\pm$ SD) and the intensity of the unfused cells tested with calcein AM was 113 ± 63 ($N = 25$ cells; mean $\pm$ SD). The intensity ratio of fused to unfused cells was $<I_{fused}>/<I_{unfused}> = 0.3$, reflecting somewhat compromised esterase activity after fusion. Nonetheless, in every single experiment, fluorescent calcein was clearly visible within the fused cells during the entire observation period, thus indicating esterase activity and an intact plasma membrane.

To gain further insight into the viability of the fused cells, we tested whether the fused cells could take up and reduce MTT to formazan as a measure of the metabolic activity in cells [27, 28]. Formation of MTT formazan in the fused cells could be easily detected as shown in Fig. 2(f) (additional experiments are shown in Fig. S2 in ESM). The increase in contrast is due to high absorption of formazan in the visible spectral region [27, 28], and we continued to observe an increase in contrast after 4 h of examination, as shown in Fig. 2(f). Therefore, we concluded that the fused syncytia can reduce MTT to formazan and additionally have active esterases. Taken together, these findings strongly suggest that the syncytia are viable with active metabolism and intact plasma membrane after the fusion event.

Cell–cell fusion has been investigated previously mostly by methods requiring an ensemble of cells [29]. Fusion of cells occurs in a vast number of biological processes and has been applied *in vitro* to basic research of cell regeneration or repair. Examples include (i) fusion of cells during tissue regeneration [29], (ii) fusion of cancer cells to different cell types including dendritic cells which are important in immune function [30], (iii) fusion of neuronal cells *in vitro* [31], (iv) fusion between transplanted bone marrow cells and hepatic cells, which induced liver regeneration [32], and (v) fusion of liposomal membranes with a cell that has a general applicability for delivering small molecules to the cytoplasm, for instance, delivery of transfecting DNA sequences, silencing RNAs, or chemical drugs.

These examples imply that fusion of cells may play an important role in biological mechanisms during a pathology and in the general cellular function. The technique presented here therefore has potential as a research technique for investigating the fusion between immune cells with cancer cells or stem cells with tissue cells, in both cases at a single-cell level. Fusion with stem cells has a therapeutic potential and can be used for tissue repair and regeneration. By monitoring the evolution of expression of pluripotency markers (like *Nanog* and *Oct4*) [33], the researcher may determine whether stand-alone specialized cells have been reprogrammed after fusion with stem cells and thereby obtained the self-regenerating properties of stem cells.

3.3 Cell–GUV fusion

By fusing a vesicle to a selected living cell, one can deliver any cargo carried by the vesicle to the cytoplasm. To perform this experiment, we made GUVs by standard electroformation and loaded them with either 300 or 200 mM sucrose. The presence of sucrose in the lumen increases the index of refraction of the GUVs with respect to the aqueous medium and thereby facilitates optical trapping of individual GUVs [18, 34]. The GUVs were stable in the hypertonic DMEM cell medium with an osmolarity of ~356 mOsmol·L^{-1}. We found that the optimal condition for cell-vesicle fusion was when a cell was locally attached to the Petri dish but the GUV was free to move in the sample; this setup was achieved by coating the Petri dishes with a mixture of 50% (v/v) gelatin (0.1%) and 50% (v/v) α-casein (2 g·L^{-1}) overnight. We never observed cell–GUV fusion when cells and vesicles were simply mixed in the chamber. Neither was fusion observed when the laser was irradiating the contact zone between a cell and a GUV, while no AuNPs were present. To increase the likelihood of having AuNPs in the contact zone between the cell and the GUV, it was useful to functionalize a fraction of the GUV lipids with biotin and to use streptavidin-coated AuNPs, thereby attaching AuNPs directly to the GUVs before the optical trap was turned on. We found that GUVs containing 200 mM sucrose undergo fusion with cells more easily than GUVs containing 300 mM sucrose do. Fusion of a cell with a vesicle happened readily using AuNPs with a diameter of only 80 nm and laser powers of 400–

750 mW in the sample. The corresponding temperature increase of the AuNPs ranges between 100 and 200 ℃ [23, 24] (above ambient temperature, which was ~37 ℃). Figure 3(a) shows images from a typical cell–GUV fusion mediated by plasmonic heating, the membrane of the vesicle is labeled by DiO (green), the cell membranes by vybrant® DiD (red), and the cytoplasm contains fluorescent calcein (green), which is the enzymatic product after enzymatic conversion from calcein AM. Upon fusion, vybrant® DiD diffuses into the membrane of the vesicle; hence, its intensity decreases as shown in Fig. 3(b). In addition, the vesicle content mixes with the cytoplasm upon fusion, and in Fig. 3(c), we quantified how calcein diffuses from the cytoplasm into the vesicle. After ~30 s, the calcein intensity remains uniform throughout the volume indicating that complete mixing has occurred.

Another example of cell–GUV fusion is shown in Fig. S3 in the ESM where a large GUV, containing smaller GUVs, undergoes fusion with a cell. After fusion, there is no membrane barrier between the lumen of the GUV and the cytoplasm; still, the smaller interior GUVs do not mix with the cytoplasm and remain in the former GUV lumen even after 80 min.
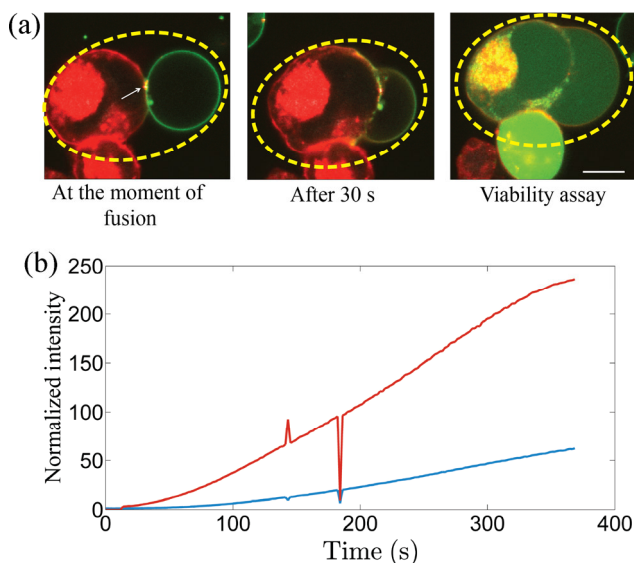
3.4 Viability after cell–GUV fusion

To investigate the viability of the fused cell–GUV structure, we used the same calcein AM assay as used to study the viability after cell–cell fusion. A sequence of images from the fusion of a green *FAST*-DiO-labeled GUV to a red vybrant® DiD-labeled HEK293 cell is shown in Fig. 4(a) (inside the yellow ellipse), where the last image displays the result of the viability experiment. Underneath the fused structure a non-fused control cell is visible. After adding calcein AM to the solution, fluorescent calcein is visible in both the fused structure and in the control cell but with higher intensity in the control cell. Figure 4(b) shows quantification of emission of calcein from the fused structure (blue trace) and in the control cell (red trace) as a function of time after addition of calcein AM to the sample. In this case, the esterase activity inside the control cell is ~fivefold stronger inside the control cell than inside the fused structure. For cell–GUV fusion, we measured
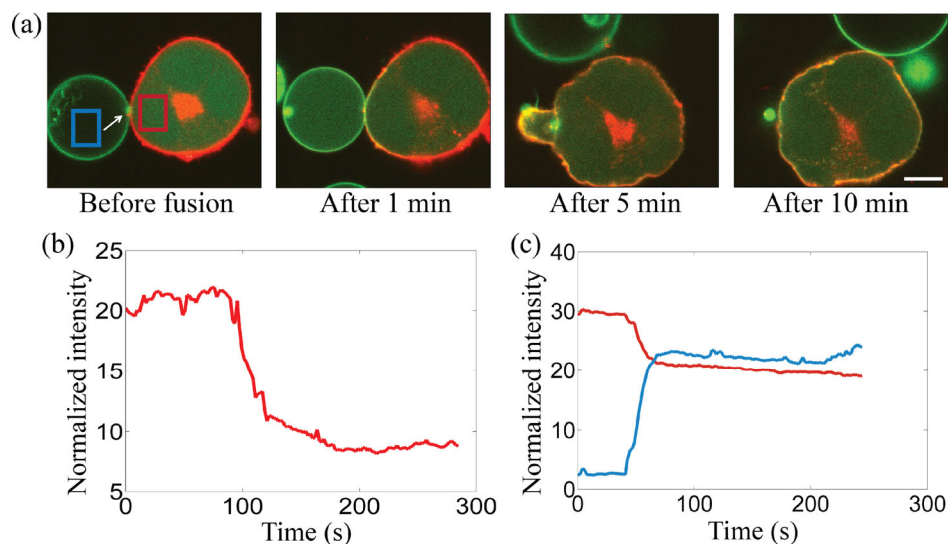
Figure 3 Hot-AuNP-mediated fusion of a live HEK293 cell with a GUV (DOPC 98.5 mol.%, biot-DSPE-PEG 1 mol.%, *FAST*-DiO 0.5 mol.%) containing 200 mM sucrose. (a) Confocal images of fusing a green (*FAST*-DiO labeled) GUV with a red (vybrant® DiD labeled) HEK293 cell. The cytoplasm of the cell is labeled with green calcein (converted from calcein AM), which diffuses into the GUV upon fusion. Laser power in the sample was $P = 750$ mW and $d_{\mathrm{AuNP}} = 80$ nm (white arrow), scale bar is 10 μm. (b) Normalized average of emitted intensities from the vybrant® DiD dye from the experiment shown in (a) as a function of time. The average pixel intensity decreases as the fluorophores diffuse over a larger membrane area. (c) Average calcein fluorescent intensity as a function of time from the two boxed regions in (a); the blue trace is from within the GUV, the red trace is from the cytoplasm. Approximately 30 s after fusion (which occurred at $t \sim 45$ s) the calcein is uniformly distributed within the fused cell–GUV structure. A total of 22 successful cell–GUV fusions were performed.

(a)

At the moment of fusion | After 30 s | Viability assay

(b)

Figure 4 Viability analysis of a cell–GUV fused structure; the original GUV (DOPC 88.5 mol.%, DOPS 10 mol.%, biot-DSPE-PEG 1 mol.%, *FAST*-DiO 0.5 mol.%) contained 200 mM sucrose. (a) Images showing hot-nanoparticle-mediated fusion between a green (*FAST*-DiO-labeled) GUV and a red (vybrant® DiD-labeled) HEK293 cell (both inside the yellow ellipse), laser power $P =$ 450 mW at sample, $d_{AuNP} = 80$ nm. Nonfluorescent calcein AM was added to the chamber 6 min after fusion, and the last image shows calcein fluorescence (a measure of esterase activity) in the fused structure as well as inside an unfused control cell (below the yellow ellipse). The scale bar is 10 μm. (b) Comparison of the calcein intensity emitted from the lumen of the fused structure (blue) and from the cytoplasm of an unfused control cell (red) as a function of time after addition of calcein AM to the chamber. The two spikes in the intensity are artefacts due to a sudden translation of the microscope stage.

the calcein signal from 3 fusions, and the intensity was 38 ± 37 (N = 3 cells; mean ± SD) and the corresponding ratio between fused and unfused cells was 0.3. Moreover, for the cell–GUV fusion, we expected a decrease in intensity due to dilution of the cytoplasm with water and sucrose delivered from the GUV.

3.5 Parameter optimization

To increase the temperature of the gold nanoparticles and thereby induce heating one can tune both the particle size and the laser power, the larger the particle or the higher the laser power, the higher the temperature [23]. We observed successful fusion events of both the cell–cell and cell–GUV assays using AuNPs in the size range between 80 and 200 nm and laser output power in the range of ~250 to 750 mW in the sample.

For each type of experiment, we optimized the parameters so that fusion would readily occur within a time scale of minutes while minimizing the laser power. If the temperature of the AuNP became too high, the cells were found to form blebs (two examples of bleb formation are shown in Fig. S4 in the ESM) or to burst (Fig. S5 in ESM). This is consistent with the results of another study where cells were exposed to prolonged local heating which led to cell blebbing caused by cortical actin contraction and local detachment of the membrane from the actin [35]. Irradiating a AuNP aggregate will cause the overall temperature to be higher than irradiating a single AuNP with the same laser power (e.g., Figs. S4(b) and S5 in the ESM). Hence, to perform controlled heating of an AuNP and obtain a successful fusion event with an intact and viable fused structure, it is desirable to prevent AuNP aggregation in the sample. PEG coating decreases the likelihood of aggregation; however, PEG is potentially toxic for live cells [36], and hence, we did not coat the particles but instead kept the AuNP concentration low to minimize the likelihood of aggregation in the trap.

The temperature at the surface of a single gold nanoparticle as well as in the surrounding medium was measured under similar conditions (but without cells) as described in Refs. [23, 24]. From these measurements, we can conclude that the temperature at a distance of 100 nm from the nanoparticle surface drops down by ca. 70% and 60% for an 80-nm AuNP and 150-nm AuNP, respectively. The maximum temperature increase at the particle surface, achieved in this work was in the range 100–200 °C. Consequently, the temperatures at a 100-nm distance from the nanoparticle surface were ~30–80 °C. This temperature range might cause local damage to both proteins and lipids, but at distances larger than 100 nm from the surface of the AuNP, the temperature continues to decay rapidly, and only minimal damage will occur. In addition, it is likely that the AuNP is displaced significantly from the center of the trap and that the temperature will be correspondingly lower. The fact that the cells still show signs of viability after fusion must indicate that the heated region surrounding the nanoparticle is sufficiently localized to avoid overall cell damage.

The choice of nanoparticles to be used for fusion significantly affects the temperature and amount of

heat stress to which the cell is exposed. The heat emitted from the particle depends on the absorption cross-section of the nanoparticle, which is known to depend on size, shape, and composition. The emitted power, q, is given by the intensity, I, (units: power/area) received by the AuNP multiplied by the absorption cross-section σ_{abs} (units: area) [37]

$$q = \sigma_{abs} \cdot I \qquad (1)$$

The simulated absorption cross-section values for AuNP with diameters of 80 and 150 nm are approximately 100 and 1,000 nm^2, respectively. In this work, we used P = 250 to 750 mW at the focal plane, and we can approximate the focal diameter to be 1 μm. If we substitute the simulated values for the absorption cross-sections and the intensities given above into Eq. (1), we will obtain emitted power in the range 0.031 to 0.096 mW for an 80-nm AuNP and from 0.3 to 1.0 mW for a 150-nm AuNP.

If the temperature of the hot AuNP was kept reasonably low and localized by avoiding trapping of large aggregates, then the syncytium was most often found to be viable after fusion. Upon fusion of a cell with a large GUV, however, we often found the viability of the newly formed structure to be compromised. One reason could be that the volume of the GUV was relatively large in comparison with the volume of the cell, even when we chose the smallest GUVs made by electroformation, to minimize the introduction of new lipids and sucrose into the cell. The GUVs contained 200–300 mM sucrose, and hence a large amount of sucrose was introduced into the cytoplasm upon fusion, and this change can reduce the enzymatic activity of the cell due to dilution of the cytoplasm. A solution to this problem could be to use smaller vesicles, possibly formed by methods other than electroformation; however, smaller vesicles are difficult to position relative to the trap because they will be localized at the center of the trap and thereby displace the AuNP [34]. Another potential solution that may be less harmful for the cells is to load the vesicles with a physiological solution [38–41] provided that the GUVs still carry sufficient refractive contrast in comparison with the medium in which they should be optically trapped.

3.6   The mechanism of cell–cell fusion

Laser-induced heating of a plasmonic AuNP located between two cells, or between a cell and a vesicle, can trigger membrane fusion. In cell–cell fusion, both cytoplasms and plasma membranes of the two cells undergo complete mixing, such that fluorophores freely diffuse both in the membrane and in the cytoplasm of the syncytium. Lumen mixing of two fusing GUVs has been shown to occur within a second [18]. This event is significantly faster than the mixing time scale of cell–cell fusion (~30 min) or cell–GUV fusion (~30 s) observed here. The viscosity of 200 mM sucrose is similar to that of water; hence, the difference in mixing time is probably due to crowding inside the cell being caused by the presence of cytoskeletal structures, the nucleus, and other subcellular organelles [42]. In addition, it takes more time for the fusion pore to expand during cell–cell or cell–GUV fusion in comparison with GUV–GUV fusion. The time scale for membrane mixing is an order of magnitude faster for GUV–GUV fusion [18] than for cell–cell or cell–GUV fusion. This difference in time scales may be caused by the fact that the cell membrane contains high concentrations of cholesterol and other lipids that cause the cellular membrane to be more closely packed and possibly organized into different physical domains, in contrast to a liquid single-phase GUV. Moreover, the presence of cortical cytoskeletal structures associated with the plasma membrane may slow down the mobility of phospholipids [43].

The mechanism of fusion is likely to involve thermal rearrangements of the membrane lipids. Fluid membranes are highly temperature sensitive and show relative area expansion of a few percent before rupturing. Several recent studies have exploited this thermal behavior of membranes for research into molecular transport [44] and gold nanoparticle transport [45, 46] across membranes or for studying phase transition phenomena [47]. Because the area of fluid membranes expands by ~0.5% per Kelvin [48], and the local temperature increase created at the site of the nanoparticle is tens of degrees, we expect the energy barrier for forming a fusion pore to be significantly lowered. Therefore, the local temperature increase may alone be responsible for triggering fusion.

4   Conclusion

Successful fusion of any two HEK293 cells of choice in a sample was performed by trapping heated gold nanoparticles at their contact region. After we positioned the cells into close proximity using an optical trap, fusion was mediated by an AuNP that diffused into the trap. The nanoparticle heated and caused full fusion of the two cells into a syncytium. Furthermore, the syncytia were tested for viability and were found to be competent at converting membrane-penetrating calcein AM into membrane-non-penetrating calcein, and additionally, the fused cells were found to be metabolically active. The cells retained the calcein in the cytoplasm after fusion, which can occur only in cells with active esterases and in cells with an intact plasma membrane; hence, the assay proves that the cell is viable with an intact membrane. On the other hand, the calcein signals measured in the viability assay were found to be lower than in unfused cells. This result could indicate some transient damage to the cell membrane or to the cytoplasm caused by the local plasmonic heating. A similar strategy was used to fuse a selected GUV to a selected cell, in this case, the newly formed structure appeared to be less viable; this phenomenon could be due to dilution of the cytoplasm by introduction of the GUV content. We expect that viability of the fused cell can be improved in the future by tweaking the size and content of the fusing GUV.

This new general method for cellular and membrane fusion is unlikely to be limited to the specific membrane composition or cell types chosen here. Various lipids and cell materials are expected to respond similarly to extreme local heating, which is the physical trigger of fusion.

The proposed fusion method offers a way to design novel cells that carry characteristics from two selected cell types or to deliver, in a controlled manner, a cargo carried by a vesicle to a selected cell, thereby implementing controlled drug delivery on the single-cell level. The method presented here provides a unique single-cell approach whereby fusion between two selected cells can be achieved and is triggered by an extremely local perturbation of the plasma membrane. Together with ongoing developments in optical manipulations like holographic trapping, we anticipate this technique to soon become highly useful in the fields of cellular design and drug delivery.

Acknowledgements

Electronic Supplementary Material: Supplementary material (additional examples of successful fusion events including MTT-viability tests, and examples of fusion events which lead to cell damage or morphological changes in cells when using large particles and high laser powers) is available in the online version of this article at http://dx.doi.org/10.1007/s12274-016-1392-3.

References

[1]   Martens, S.; McMahon, H. T. Mechanisms of membrane fusion: Disparate players and common principles. *Nat. Rev. Mol. Cell Biol.* **2008**, *9*, 543–556.

[2]   Chen, Y. A.; Scheller, R. H. SNARE-mediated membrane fusion. *Nat. Rev. Mol. Cell Biol.* **2001**, *2*, 98–106.

[3]   Pérez-Vargas, J.; Krey, T.; Valansi, C.; Avinoam, O.; Haouz, A.; Jamin, M.; Raveh-Barak, H.; Podbilewicz, B.; Rey, F. A. Structural basis of eukaryotic cell-cell fusion. *Cell* **2014**, *157*, 407–419.

[4]   Brouwer, I.; Giniatullina, A.; Laurens, N.; van Weering, J. R. T.; Bald, D.; Wuite, G. J. L.; Groffen, A. J. Direct quantitative detection of Doc2b-induced hemifusion in optically trapped membranes. *Nat. Commun.* **2015**, *6*, 8387.

[5]   Weber, T.; Zemelman, B. V.; McNew, J. A.; Westermann, B.; Gmachl, M.; Parlati, F.; Söllner, T. H.; Rothman, J. E. SNAREpins: Minimal machinery for membrane fusion. *Cell* **1998**, *92*, 759–772.

[6]   Floyd, D. L.; Ragains, J. R.; Skehel, J. J.; Harrison, S. C.; van Oijen, A. M. Single-particle kinetics of influenza virus membrane fusion. *Proc. Natl. Acad. Sci. USA* **2008**, *105*, 15382–15387.

[7] Estes, D. J.; Lopez, S. R.; Fuller, A. O.; Mayer, M. Triggering and visualizing the aggregation and fusion of lipid membranes in microfluidic chambers. *Biophys. J.* **2006**, *91*, 233–243.

[8] Longo, M. L.; Waring, A. J.; Hammer, D. A. Interaction of the influenza hemagglutinin fusion peptide with lipid bilayers: Area expansion and permeation. *Biophys. J.* **1997**, *73*, 1430–1439.

[9] Chakraborty, H.; Mondal, S.; Sarkar, M. Membrane fusion: A new function of non steroidal anti-inflammatory drugs. *Biophys. Chem.* **2008**, *137*, 28–34.

[10] Ohki, S. Effects of divalent cations, temperature, osmotic pressure gradient, and vesicle curvature on phosphatidylserine vesicle fusion. *J. Membr. Biol.* **1984**, *77*, 265–275.

[11] Wilschut, J.; Duezguenes, N.; Papahadjopoulos, D. Calcium/magnesium specificity in membrane fusion: Kinetics of aggregation and fusion of phosphatidylserine vesicles and the role of bilayer curvature. *Biochemistry* **1981**, *20*, 3126–3133.

[12] van Lengerich, B.; Rawle, R. J.; Bendix, P. M.; Boxer, S. G. Individual vesicle fusion events mediated by lipid-anchored DNA. *Biophys. J.* **2013**, *105*, 409–419.

[13] Rawle, R. J.; van Lengerich, B.; Chung, M.; Bendix, P. M.; Boxer, S. G. Vesicle fusion observed by content transfer across a tethered lipid bilayer. *Biophys. J.* **2011**, *101*, L37–L39.

[14] Haluska, C. K.; Riske, K. A.; Marchi-Artzner, V.; Lehn, J. M.; Lipowsky, R.; Dimova, R. Time scales of membrane fusion revealed by direct imaging of vesicle fusion with high temporal resolution. *Proc. Natl. Acad. Sci. USA* **2006**, *103*, 15841–15846.

[15] Saito, A. C.; Ogura, T.; Fujiwara, K.; Murata, S.; Nomura, S.-I. M. Introducing micrometer-sized artificial objects into live cells: A method for cell–giant unilamellar vesicle electrofusion. *PLoS One* **2014**, *9*, e106853.

[16] Robinson, T.; Verboket, P. E.; Eyer, K.; Dittrich, P. S. Controllable electrofusion of lipid vesicles: Initiation and analysis of reactions within biomimetic containers. *Lab Chip* **2014**, *14*, 2852–2859.

[17] Yeheskely-Hayon, D.; Minai, L.; Golan, L.; Dann, E. J.; Yelin, D. Optically induced cell fusion using bispecific nanoparticles. *Small* **2013**, *9*, 3771–3777.

[18] Rørvig-Lund, A.; Bahadori, A.; Semsey, S.; Bendix, P. M.; Oddershede, L. B. Vesicle fusion triggered by optically heated gold nanoparticles. *Nano Lett.* **2015**, *15*, 4183–4188.

[19] Bendix, P. M.; Jauffred, L.; Norregaard, K.; Oddershede, L. B. Optical trapping of nanoparticles and quantum dots. *IEEE J. Sel. Top. Quant.* **2014**, *20*, 4800112.

[20] Richardson, A. C.; Reihani, N.; Oddershede, L. B. Combing

confocal microscopy with precise force-scope optical tweezers. In *Proceedings of SPIE 6326, Optical Trapping and Optical Micromanipulation III*, San Diego, California, USA, 2006.

[21] Reihani, S. N. S.; Mir, S. A.; Richardson, A. C.; Oddershede, L. B. Significant improvement of optical traps by tuning standard water immersion objectives. *J. Opt.* **2011**, *13*, 105301.

[22] Hansen, P. M.; Bhatia, V. K.; Harrit, N.; Oddershede, L. Expanding the optical trapping range of gold nanoparticles. *Nano Lett.* **2005**, *5*, 1937–1942.

[23] Bendix, P. M.; Reihani, S. N. S.; Oddershede, L. B. Direct measurements of heating by electromagnetically trapped gold nanoparticles on supported lipid bilayers. *ACS Nano* **2010**, *4*, 2256–2262.

[24] Kyrsting, A.; Bendix, P. M.; Stamou, D. G.; Oddershede, L. B. Heat profiling of three-dimensionally optically trapped gold nanoparticles using vesicle cargo release. *Nano Lett.* **2011**, *11*, 888–892.

[25] Kaneshiro, E. S.; Wyder, M. A.; Wu, Y.-P.; Cushion, M. T. Reliability of calcein acetoxy methyl ester and ethidium homodimer or propidium iodide for viability assessment of microbes. *J. Microbiol. Meth.* **1993**, *17*, 1–16.

[26] Gatti, R.; Belletti, S.; Orlandini, G.; Bussolati, O.; Dall'Asta, V.; Gazzola, G. C. Comparison of annexin V and calcein-AM as early vital markers of apoptosis in adherent cells by confocal laser microscopy. *J. Histochem. Cytochem.* **1998**, *46*, 895–900.

[27] Stockert, J. C.; Blázquez-Castro, A.; Cañete, M.; Horobin, R. W.; Villanueva, Á. MTT assay for cell viability: Intracellular localization of the formazan product is in lipid droplets. *Acta Histochem.* **2012**, *114*, 785–796.

[28] Liu, Y.; Peterson, D. A.; Kimura, H.; Schubert, D. Mechanism of cellular 3-(4,5-dimethylthiazol-2-yl)-2,5-diphenyltetrazolium bromide (MTT) reduction. *J. Neurochem.* **1997**, *69*, 581–593.

[29] Ogle, B. M.; Cascalho, M.; Platt, J. L. Biological implications of cell fusion. *Nat. Rev. Mol. Cell Biol.* **2005**, *6*, 567–575.

[30] Gong, J. L.; Nikrui, N.; Chen, D. S.; Koido, S.; Wu, Z. K.; Tanaka, Y.; Cannistra, S.; Avigan, D.; Kufe, D. Fusions of human ovarian carcinoma cells with autologous or allogeneic dendritic cells induce antitumor immunity. *J. Immunol.* **2000**, *165*, 1705–1711.

[31] Giordano-Santini, R.; Linton, C.; Hilliard, M. A. Cell-cell fusion in the nervous system: Alternative mechanisms of development, injury, and repair. *Semin. Cell Dev. Biol.*, in press, DOI: 10.1016/j.semcdb.2016.06.019.

[32] Vassilopoulos, G.; Wang, P. R.; Russell, D. W. Transplanted bone marrow regenerates liver by cell fusion. *Nature* **2003**, *422*, 901–904.

[33] Jang, H. S.; Hong, Y. J.; Choi, H. W.; Song, H.; Byun, S. J.; Uhm, S. J.; Seo, H. G.; Do, J. T. Changes in parthenogenetic imprinting patterns during reprogramming by cell fusion. *PLoS One* **2016**, *11*, e0156491.

[34] Bendix, P. M.; Oddershede, L. B. Expanding the optical trapping range of lipid vesicles to the nanoscale. *Nano Lett.* **2011**, *11*, 5431–5437.

[35] Oyama, K.; Arai, T.; Isaka, A.; Sekiguchi, T.; Itoh, H.; Seto, Y.; Miyazaki, M.; Itabashi, T.; Ohki, T.; Suzuki, M. et al. Directional bleb formation in spherical cells under temperature gradient. *Biophys. J.* **2015**, *109*, 355–364.

[36] Biondi, O.; Motta, S.; Mosesso, P. Low molecular weight polyethylene glycol induces chromosome aberrations in Chinese hamster cells cultured *in vitro*. *Mutagenesis* **2002**, *17*, 261–264.

[37] Baffou, G.; Berto, P.; Bermúdez Ureña, E.; Quidant, R.; Monneret, S.; Polleux, J.; Rigneault, H. Photoinduced heating of nanoparticle arrays. *ACS Nano* **2013**, *7*, 6478–6488.

[38] Pott, T.; Bouvrais, H.; Méléard, P. Giant unilamellar vesicle formation under physiologically relevant conditions. *Chem. Phys. Lipids* **2008**, *154*, 115–119.

[39] Estes, D. J.; Mayer, M. Giant liposomes in physiological buffer using electroformation in a flow chamber. *Biochim. Biophys. Acta* **2005**, *1712*, 152–160.

[40] Montes, L. R.; Alonso, A.; Goñi, F. M.; Bagatolli, L. A. Giant unilamellar vesicles electroformed from native membranes and organic lipid mixtures under physiological conditions. *Biophys. J.* **2007**, *93*, 3548–3554.

[41] Weinberger, A.; Tsai, F.-C.; Koenderink, G. H.; Schmidt, T. F.; Itri, R.; Meier, W.; Schmatko, T.; Schröder, A.; Marques, C. Gel-assisted formation of giant unilamellar vesicles. *Biophys. J.* **2013**, *105*, 154–164.

[42] Luby-Phelps, K. Cytoarchitecture and physical properties of cytoplasm: Volume, viscosity, diffusion, intracellular surface area. *Int. Rev. Cytol.* **2000**, *192*, 189–221.

[43] Fujiwara, T.; Ritchie, K.; Murakoshi, H.; Jacobson, K.; Kusumi, A. Phospholipids undergo hop diffusion in compartmentalized cell membrane. *J. Cell Biol.* **2002**, *157*, 1071–1082.

[44] Andersen, T.; Kyrsting, A.; Bendix, P. M. Local and transient permeation events are associated with local melting of giant liposomes. *Soft Matter* **2014**, *10*, 4268–4274.

[45] Li, M.; Lohmuller, T.; Feldmann, J. Optical injection of gold nanoparticles into living cells. *Nano Lett.* **2015**, *15*, 770–775.

[46] McDougall, C.; Stevenson, D. J.; Brown, C. T. A.; Gunn-Moore, F.; Dholakia, K. Targeted optical injection of gold nanoparticles into single mammalian cells. *J. Biophotonics* **2009**, *2*, 736–743.

[47] Andersen, T.; Bahadori, A.; Ott, D.; Kyrsting, A.; Reihani, S. N.; Bendix, P. M. Nanoscale phase behavior on flat and curved membranes. *Nanotechnology* **2014**, *25*, 505101.

[48] Pan, J. J.; Heberle, F. A.; Tristram-Nagle, S.; Szymanski, M.; Koepfinger, M.; Katsaras, J.; Kučerka, N. Molecular structures of fluid phase phosphatidylglycerol bilayers as determined by small angle neutron and X-ray scattering. *Biochim. Biophys. Acta* **2012**, *1818*, 2135–2148.